

Deep-Learning Model for Wheat Disease and Pest Classification

Lakshmi Priya S, R Subhashini

Cite as Priya S, L., & Subhashini, R. (2024). Deep-Learning Model for Wheat Disease and Pest Classification. International Journal of Microsystems and IoT, 2(5), 871-880.

<https://doi.org/10.5281/zenodo.13132457>




© 2024 The Author(s). Published by Indian Society for VLSI Education, Ranchi, India



Published online: 15 May 2024.



Submit your article to this journal: 




Article views: 



View related articles: 



View Crossmark data: 

DOI: <https://doi.org/10.5281/zenodo.13132457>

Full Terms & Conditions of access and use can be found at <https://ijmit.org/mission.php>



Deep-Learning Model for Wheat Disease and Pest Classification



Lakshmi Priya S¹, R Subhashini²

¹Department of Computer Science and Engineering, ²Department of Information Technology,
^{1,2}Sathyabama Institute of Science and Technology, Chennai, India.

ABSTRACT

Severe pests and diseases in wheat are caused by global change and natural disturbances. This results in a significant loss of yield and quality. Therefore, ecological problems will be solved by early detection of diseases and pests. In prevailing techniques, different types of wheat diseases and pests were not studied completely. Hence, a Deep-Learning (DL) framework for wheat field disease and pest classification in leaves via satellite images using Non-monotonic Correlated-Extreme Learning Machine (NC-ELM) is proposed. Primarily, the farm field's satellite images are given as input to the proposed framework. Afterward, to remove unwanted noises, the images are pre-processed using Wavelet Spearmann Rank Transform (WSRT). Next, by utilizing the Adaptive Irregular SegNet (AIS) algorithm, the leaf regions are segmented. Then, to separate patches, the slicing of images is evaluated. After that, the graph is constructed via the Cosine Similarity induced Kruskal's Minimum Spanning Tree (CSK-MST) algorithm. Here, the pests are indicated in highlighted points; then, the features are extracted. Moreover, the features are extracted from the other regions. The optimal features are selected from the extracted features using the Parallel Group Gazelle Optimization Algorithm (PG-GOA). Lastly, the resultant optimal features are fed into the NC-ELM classifier. Hence, NC-ELM classifies pests and diseases. Experiments were conducted for the proposed technique with the conventional approaches, which proved the proposed one's efficacy.

KEYWORDS

Wavelet Spearmann Rank Transform (WSRT), Adaptive Irregular SegNet (AIS), Cosine Similarity induced Kruskal's minimum spanning tree (CSK-MST) algorithm, Parallel Group Gazelle Optimization Algorithm (PG-GOA), and Non-monotonic Correlated-Extreme Learning Machine (NC-ELM).

1. INTRODUCTION

Globally, the second most significant food resource is wheat. It plays a critical role in supporting worldwide food security, which represents the world's highest producer [1]. In 2050, the global population is predicted to be 9 billion, which meets the expected augmented demand of 60 percent. The annual wheat yield needs to increase from the present level of 1% to at least 1.6% [2]. Thus, the agricultural forecast output is exceeded by the projected demand for cereal grain. For satisfying the projected worldwide food demand, global crop production must be doubled. Despite the crops' consumptive water usage, pests and diseases could limit the yields since they interrupt significant physiological processes, such as respiration, nutrient translocation, photosynthesis, water, et cetera [3]. Pests mainly occur in the leaf part of a plant. The Leaf Area Index (LAI) is used for calculating biophysical processes in crop models.

Hence, during the entire growing season, this parameter's persistent monitoring is significant for farm management [4]. Some of the pests and diseases are given as follows. One of the economically significant insect pests is the Orange Wheat Blossom Midge (OWBM). In Canada as well as the UK, OWBM caused annual wheat losses exceeding C\$60,000,000 and £60,000,000, correspondingly [5].

Currently, the most destructive and prevalent rust pathogen in wheat is leaf rust, which is caused by the obligate biotrophic fungus. For disturbing spike formation or else making the spike partly or entirely bleached, the rachis's base or upper part is generally attacked by the wheat blast pathogen, which leads to wrinkled seeds or no grain [6] [7]. Therefore, the detection of pests and diseases is more significant.

Hence, manual techniques are introduced. This is also limited concerning the higher rate of manual errors, accuracy, together with time consumption. For enhancing the physiological trait prediction using wheat leaf reflectance spectral data, various Machine Learning (ML) systems are utilized [8] [9]. Pest and disease classification is vital for crop disease detection, with the DL technology development in current years. Thus, for collecting higher-resolution images, satellite, airplane, and on-ground machinery platforms have been adopted by various studies. But, regarding spatial resolutions, numerous limitations are faced by airplane and satellite technologies. Also, they render an expensive solution [10]. As per various reports, the sensitive bands screened by remote sensing are diverse. Hence, a DL framework for wheat field disease and pest classification in leaves via satellite images using NC-ELM is proposed.

1.1 Problem Statement

Some of the existing techniques have some disadvantages, which are described below,

- Wheat disease detection was generally described using RGB images; also, the irregular and blurred boundary problems of the areas are not considered by the basic semantic segmentation algorithms, which restricted the disease segmentation performance.
- In existing techniques, satellite image-based wheat field analyses concentrated on a particular type of wheat disease. Different types of wheat field diseases were not studied.
- The classification of both the pests and the diseases was not done in most of the existing methodologies.

1.2 Objectives

The proposed research system has some research objectives, which are enlisted further,

- ❖ The proposed model develops an automatic wheat disease and pest classification algorithm using satellite images to cope with boundary problems.
- ❖ To overcome the field's irregular as well as blurred boundary problems, a region segmentation AIS algorithm is proposed, which resulted in an accurate segmentation.
- ❖ An effective NC-ELM classification algorithm is modeled to classify different types of wheat field diseases and pests.

The paper is organized as: the associated works are elucidated in Section 2; the proposed methodology is illustrated in Section 3; the experimental perusal is demonstrated in Section 4; lastly, the paper is wrapped up in Section 5.

2. RELATED WORKS

An effective Dual Flow UNet (DF-UNet) detection algorithm for predicting various levels of diseases was recommended. As per the outcome, the Overall Accuracy (OA) on yellow rust detection reached 96.93%. But, it was challenging to detect yellow rust at an earlier stage, thus less labeled data was required [11].

A detection technique that was named a specific Fusarium Head Blight (FHB) was presented. Here, a system, which combined the Instability Index and Spectral Angle Mapper classifier (ISI-SAM), was wielded. An overall classification accuracy (89.80%) was attained by the developed approach. The limitation here was the presented technique utilized a lower sampling quantity in every single stage [12].

A model for the Yellow Rust Optimal Index (YROOI) was established. This model was designed using hyperspectral data, which was wielded by a spectrometer for quantitatively estimating yellow rust. Outcomes demonstrated a higher accuracy for the presented technique. The model was not validated using imagery even though it yielded optimal outcomes in ground-centric hyperspectral data. Hence, it was not suitable for imagery data [13].

A model of disease severity concerning fusion features of the image and spectral features was designed. Here, twelve sensitive bands were extracted. The accuracy attained by the training and prediction set was 95% and 92%, correspondingly. The presented technique utilized only some factors; thus, it was not feasible to achieve the accurate identification of diseases and classification of pests [14].

A model for mapping protocol using wheat rust disease was proffered. Here, non-vegetated as well as lodged areas were deleted; also, the vegetation indices were filtered. An accuracy of 93.60% was attained by the presented wrapper feature selection system. The developed system had an issue with binary classification owing to the limitation of the sample with healthy and rust wheat [15].

An ML approach for predicting the risk levels in one or more mycotoxins in wheat on a regional basis in Europe was recommended. The internal and external validation led to 0.90–0.99 prediction accuracy. The presented method utilized some satellite images for the working process, thus it was not reliable for many images [16].

A model for detecting diseased areas using wheat spikes' color images was propounded. For the dataset, shadow condition images were collected using wheat spikes' color images at the milk stage. The model was evaluated; also, the mean Average Precision (mAP) for the testing dataset was 0.9201. The presented method attained low accuracy since it utilized a narrow range of the dataset [17].

A model for the wheat mildew impact in stored food, and demonstrated that it was utilized for the detection of mildew and also viable to use WiFi Channel State Information (CSI) amplitude in stored wheat was introduced. An average accuracy of 90% was attained by the presented mechanism. The presented method faced the challenges of dynamic environments and human influence [18].

An accurate and sensitive technique for detecting MoT at the seedling and vegetative stages for disease control was established. The presented technique was easily adapted for rapidly detecting wheat blasts and other significant plant diseases in the field. The presented method utilized a single Polymerase Chain Reaction (PCR) in which only low sequences were allowed, thus it was not feasible for large sequences [19].

An efficient data augmentation strategy for the CNN-centric mechanism was developed. The presented technique adopted data augmentation via rotating images by several degrees. The

detection's effects were enhanced by the presented method's test time augmentation when contrasted with the single-scale detection. The presented technique obtained low pest detection performances of 81.4% mAP [20].

3. PROPOSED WHEAT DISEASE AND PEST CLASSIFICATION USING NC-ELM

The agriculture production's focus is a stable as well as higher yield of wheat. To achieve this goal, it is significant to detect diseases and pests timely and effective. For that, a DL framework for wheat field disease and pest classification in leaves via satellite images is developed using NC-ELM. Figure 1 elucidates the proposed mechanism's block diagram.

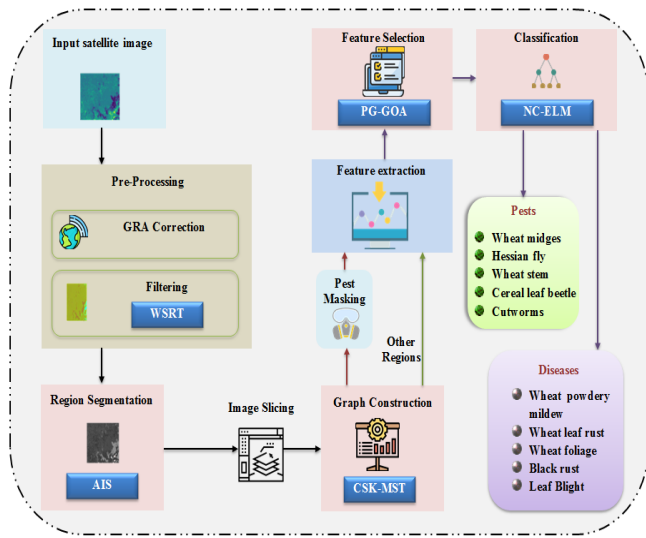


Figure 1: Block diagram for the proposed deep-learning framework for the classification of wheat disease and pest

3.1 Input

Primarily, satellite images from the wheat farm field are collected. Therefore, the inputs (S) are mathematically represented as,

$$S = \{S_1, S_2, S_3, S_4, \dots, S_u\} \text{ or } S_t, t = 1, 2, 3, 4, \dots, u \quad (1)$$

Where, S_t signifies the inputs and t epitomizes the u number of satellite images of wheat.

3.2 Pre-Processing

Here, the pre-processing processes, such as Geometric, Radiometric, and Atmospheric (GRA) are executed; also, filtering is performed to remove the noises.

3.2.1 GRA correction

In this subphase, GRA correction is detailed. Here, atmospheric correction is computed for detecting clouds along with their shadows on the ground and for correcting perturbations in connection with aerosol effects. Radiometric correction is utilized to remove spectral distortions in the data. Geometric correction is evaluated to clear the positional errors in the image. They are mathematically denoted as,

$$\tau^0 a(dB) = 20 \times \log_{10}(\gamma a) + 10 \times \log_{10}(M) \times \log_{10}(\sin(\mu a)) \quad (2)$$

$$\tau^0 a(dB) = 20 \times \log_{10}\left(\frac{\gamma a}{H2a}\right) + 10 \times \log_{10}(\sin(\mu a)) \quad (3)$$

$$\tau^0 a(dB) = 20 \times \log_{10}(\gamma a) + M \quad (4)$$

Where, τ^0 signifies the backscattering coefficient at the pixel (a), γ is the wavelength's digital number, M is the calibration constant, $H2$ is the gain, and μ is the incidence angle. Thus, the output is signified as ζ .

3.2.2 Filtering

The GRA correction output (ζ) is given for the filtering process. To remove the noises present in the satellite images, filtering is done using WSRT. WT preserves the crucial features and also removes the non-important components. Here, threshold values are selected manually in a general wavelet model. Thus, Spearman Rank (SR) correlation is calculated for image pixels. The maximum correlation of the image is considered as a threshold value. Generally, the expression for the Wavelet Transform (WT) (\mathfrak{S}) is given by,

$$\mathfrak{S}_{(b,c)}(h) = \frac{1}{\sqrt{c}} \mathfrak{S}\left(\frac{h-b}{c}\right) \quad (5)$$

Where, c signifies the scaling, b symbolizes the translation, and h implies the time period. Using (\mathfrak{S}), wavelet coefficient (λ) is expressed as,

$$\lambda = \mathfrak{S}\{\zeta\} \quad (6)$$

The coefficients are tuned using a suitable threshold value. Here, the tuned thresholded wavelet coefficients are selected using SR (ϖ), which is given by,

$$\varpi = 1 - \frac{6 \sum g}{p(p-1)} \quad (7)$$

Where, g is the distance betwixt two images and p signifies the number of images. Now, the Inverse WT (IWT) is applied on the tuned thresholded wavelet coefficients, which provides a noise-free image. Therefore, the pre-processed images are exemplified as \mathcal{G} .

3.3 Region Segmentation

The pre-processed images (\mathcal{G}) are given to the region segmentation phase. Here, by utilizing the AIS, only the field region is segmented by neglecting the unwanted regions. The SegNet comprises a down-sampling path as well as an up-sampling path, followed by a final pixel-wise classification layer. However, the field area's irregular and blurred boundary problems are not considered by this prevailing segmentation model. To mitigate such limitations, the Irregular Encoder Module (IEM) is introduced for getting an irregular object's feature, which is wielded for attaining a more accurate segmentation outcome. Also, Irregular Decoder Module (IDM) is applied as an upsampling module in the decoder for replacing the original one in SegNet. Along with IDM, adaptive kernels are generated for every single target location as per its content and then reassemble with predicted kernels. The structure for the AIS is given as follows.

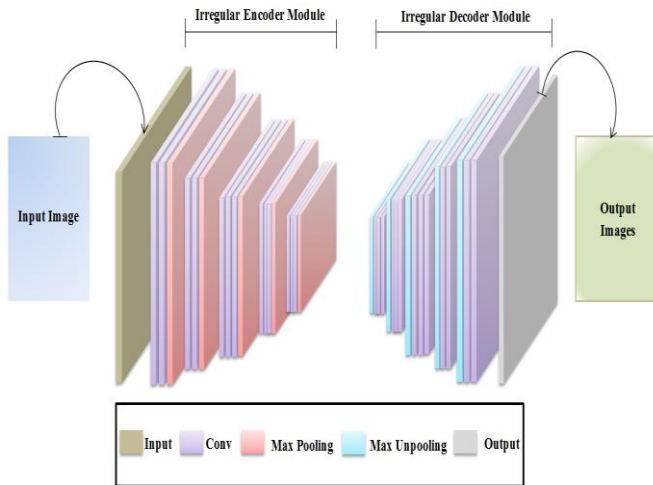


Figure 2: Architecture for AIS

SegNet comprises convolutional layers, a maximum pooling layer, and a max unpooling layer. The pre-processed images undergo encoding. The expression for encoding using IEM $\{\wp(v_0)\}$ is given as,

$$\wp(v_0) = \sum_{v_n \in \mathcal{G}} M(v_n) \cdot f(v_0 + v_n + \Delta v_n) \quad (8)$$

Where, $\wp(\)$ is the encoded output, $M(\)$ signifies the corresponding weight, Δv_n represents the learnable parameter, and n implies the pre-processed images' position.

Thus, the encoded output is given to the convolutional layer, which is expressed as,

$$\xi = \max \left(0, \sum_{n=1}^N \wp(v_0) * w \right) \quad (9)$$

Where, ξ specifies the convolutional layer's output, N implies the total number of images, and w notates the kernel function. Afterward, it is given to the max pooling layer, which lowers the image dimensionality by lowering the number of pixels in the output from the prior convolutional layer (ξ). Now, it undergoes max unpooling layer. Therefore, the output is notated as (ξ_{up}). Then, the process of decoding takes place. Here, IDM(β) is utilized for calculating parameter, which is given as,

$$Par(\beta) = \xi_{up} \times C_z + C_z \times U^2 \times K_{up}^2 \times K_{encoding}^2 \quad (10)$$

Where, $Par(\)$ is the parameter calculation, C_z , U , K_{up}^2 and $K_{encoding}^2$ represent the compressed channel, up ratio, convolutional layer's kernel size, and the generated kernel's size, correspondingly. Thus, the output of the region segmentation phase is mathematically symbolized as ψ .

3.4 Image Slicing

The output of the region segmentation phase (ψ) is given as input to the image-slicing phase. Here, the images are sliced into separate patches for the effective detection of pests and diseases. Slicing reduces workloads and data storage space requirements. The sliced images are represented as φ .

3.5 Graph Construction

The sliced images (φ) are given for constructing the graph. Here, to distinguish the wheat fields into pest regions and other regions, graph-based image segmentation is done using CSK-MST. Image segmentation-based MST is a fast and efficient technique to produce a set of segments of an image. The benefit of the algorithm is to find similar structures within clusters. In existing MST, if the clustering is performed, the pixel values that are in the same cluster attain high difference values. Therefore, the number of segments was not accurate. Hence, to overcome that, the cosine similarity weighted edge is detected. It is used for finding an exact number of segments. Primarily, arrange all the edges of the given graph and let it be $\hat{h}(L, Z)$ in non-decreasing order as per their edge weight. Compute the cluster head with the help of clusters. The cosine similarity (\mathcal{S}) between two pixels i and j is given as,

$$\aleph = \frac{\vec{\varphi}_i \cdot \vec{\varphi}_j}{\|\vec{\varphi}_i\| \|\vec{\varphi}_j\|} \quad (11)$$

Where, $\vec{\varphi}_i$ symbolizes the cosine angle of the i image pixel, and $\vec{\varphi}_j$ specifies the cosine angle of the j image pixel. Check whether the cosine similarity forms a cycle with the spanning tree. If there is no cycle, include this edge to the spanning tree, else discard it. The steps are continued until the number of edges is left in the spanning tree. Using the spanning tree, a graph is constructed with vertices as input frame pixels (φ) and edges as the color differences among 2 adjacent vertices, l_i and l_j as,

$$E(l_i, l_j) = \|\varphi(l_i) - \varphi(l_j)\| \quad (12)$$

Where, $E(\)$ signifies the constructed graph. Primarily, the graph is executed with every single vertex l_i in its component (L_i); also, the edges are arranged in the ascending weight of E . By utilizing graph construction, region merging $N(L_1, L_2)$ among L_1 and L_2 is calculated. The region merging of two components is given by,

$$N(L_1, L_2) = \begin{cases} True & .if D_{if}(L_1, L_2) > PInn(L_1, L_2) \\ False & .Otherwise \end{cases} \quad (13)$$

$$D_{if}(L_1, L_2) = \min_{l_i \in L_1, l_j \in L_2, (l_i, l_j) \in Z} E(l_i, l_j) \quad (14)$$

$$PInn(L_1, L_2) = \min(Inn(L_1) + (L_1), Inn(L_2) + (L_2)) \quad (15)$$

$$Inn(L) = \max_{x \in h(L, Z)} E(x) \quad (16)$$

Where, $D_{if}(L_1, L_2)$ is the difference among the components, $Inn(L_1, L_2)$ signifies the inner difference with no less than one of the components, and Z denotes the edges that match the neighboring vertices. $h(L, Z)$ signifies the component L 's minimum spanning tree. Here, the pests' points are highlighted by employing graph construction. Therefore, the output is mathematically notated as ϕ . From the constructed graph (ϕ), the pests and the other regions are segmented. Next, masking is performed for the pests.

3.6 Feature Extraction

The output of the constructed graph (ϕ) is given as input to the feature extraction phase. Here, features are extracted from the masked pests and also from the other regions.

3.6.1 Pests features

Some of the features like texture (K_1), color (K_2), shape (K_3), Histogram of Gradient (HoG) (K_4), Gradient Info (GIST) (K_5), dimension (K_6), shape (K_7), size (K_8), GLCM features (K_9), Normalized Difference Vegetation Index (NDVI) (K_{10}), Soil Adjusted Vegetation Index (SAVI) (K_{11}), Enhanced Vegetation Index (EVI) (K_{12}), Normalized Difference Texture Indices (NDTI) (K_{13}), RedEdge NDVI (K_{14}), and Modified Simple Ratio (MSR) (K_{15}) are extracted from the pests.

3.6.2 Features from other regions

In addition to pests features [$K_{10}, K_{11}, K_{12}, K_{13}, K_{14}$ and K_{15}], features from other regions, such as Green NDVI (K_{16}), Powdery Mildew Index (PMI) (K_{17}), Photochemical Reflectance Index (PRI) (K_{18}), Photosynthetic Radiation Index (PRI) (K_{19}), Modified Chlorophyll Absorption Ratio Index (MCARI) (K_{20}), Anthocyanin Reflectance Index (ARI) (K_{21}), Normalized Powdery Mildew Index (NPMI) (K_{22}), Ratio PMI (K_{23}), YROI (K_{24}), Green Index (K_{25}), and Green Leaf Index (K_{26}) are also extracted.

The total extracted features (K_e) are expressed as,

$$K_e = \{K_1, K_2, K_3, \dots, K_{26}\} \quad (17)$$

Where, e symbolizes the number of features.

3.7 Feature Selection

For selecting optimal features, the extracted features (K_e) are inputted into the feature selection phase. Here, PG-GOA is utilized for selecting optimal features. GOA is inspired by the gazelles' survival capability in their predator-dominated environment. In the predator's absence, the gazelles graze peacefully in the algorithm's exploratory phase. Once the predator gets spotted, the GOA goes into the exploitation stage that comprises gazelle outrunning as well as outmaneuvering. But, all the gazelle individuals gather together once the optimal position is determined, thus weakening the population diversity. The indi-

vidual gazelle in the population tends to be consistent by making the search process easier to fall into a local optimum. Hence, for enhancing the algorithm's solution quality, a parallel search strategy and group cooperation strategy are developed. The parallel search strategy determines multiple center locations in the iterative process for improving the global search ability of the algorithm. A group cooperation strategy improves the model with the help of communication between group members, which improves search efficiency.

Let us consider the extracted features as gazelles. Initialize the population of the gazelles as $Pop(K_e)$. Compute the fitness. Here, maximum accuracy is considered as fitness. The expression for fitness (μ_c) is given as,

$$\mu_c = \max(acc) \quad (18)$$

Where, acc symbolizes accuracy. Food is searched by the parallel search strategy (P_{ss}), which then compares the optimal solutions of every single gazelle for determining the global optimal solution, which is given by,

$$P_{ss}^{search} \rightarrow S_e \quad (19)$$

Where, S_e symbolizes the parameter for food. Here, the PG-GOA is performed in two ways: exploitation and exploration phase.

a) Exploitation phase

The gazelles are assumed to be peacefully grazing in the absence of a predator. Thus, assume that the gazelles move in Brownian motion while grazing. It is mathematically represented as,

$$\vec{\mathcal{E}}_{e+1} = \vec{\mathcal{E}}_e + l \cdot \vec{T} * \vec{T}_B * (\vec{F}_e - \vec{T}_B * \vec{\mathcal{E}}_e) \quad (20)$$

Where, $\vec{\mathcal{E}}_{e+1}$ is the solution of the next iteration, $\vec{\mathcal{E}}_e$ is the solution at the current iteration, l signifies the gazelles' grazing speed, \vec{T}_B specifies a vector, which contains random numbers representing the Brownian motion (B), and \vec{T} is a vector of uniform random numbers.

b) Exploration phase

This phase kicks off at the Brownian motion moment and then a predator is sighted. The gazelle's behavior once it spots the predator is given by,

$$\vec{\mathcal{E}}_{e+1} = \vec{\mathcal{E}}_e + S_p \cdot \varpi \cdot \vec{T} * \vec{T}_{Ly} * (\vec{F}_e - \vec{T}_{Ly} * \vec{\mathcal{E}}_e) \quad (21)$$

Wherein, the top speed the gazelle can reach is specified as S_p , and a vector of random numbers grounded on Lévy distributions (Ly) is signified as \vec{T}_{Ly} . The behavior of the predator chasing the gazelle is mathematically expressed as,

$$\vec{\mathcal{E}}_{e+1} = \vec{\mathcal{E}}_e + S_p \cdot \varpi \cdot \chi_{CF} * \vec{T}_{Ly} * (\vec{F}_e - \vec{T}_{Ly} * \vec{\mathcal{E}}_e) \quad (22)$$

Here, χ_{CF} represents the parameter that controls the movement of the predator. The gazelle's ability to escape is affected by the Predator Success Rates (PSRs). The PSRs effect is modeled as,

$$\vec{\mathcal{E}}_{e+1} = \begin{cases} \vec{\mathcal{E}}_e + \chi_{CF} [\vec{\eta} + \vec{T} * (\vec{\alpha} - \vec{\eta})] * \vec{U} & , \text{if } h \leq \aleph_{psr} \\ \vec{\mathcal{E}}_e + [\aleph_{psr} (1-h) + h] [\vec{\mathcal{E}}_{h_1} - \vec{\mathcal{E}}_{h_2}] & , \text{else} \end{cases} \quad (23)$$

Wherein, \vec{U} represents a binary vector, h epitomizes the random number, \aleph_{psr} symbolizes the PSR, h_1 and h_2 are gazelle matrix's random indexes. The best-obtained solution is updated with the help of grouping cooperation strategy (t) to improve the process using communication expression, which is given by,

$$t = \begin{cases} V_e^{th} & , \text{if } t = \text{current} \\ (V - t + 1)^{th} & , \text{if } t = 1, 2, \dots, V/2 \end{cases} \quad (24)$$

Where, V_e^{th} signifies the V^{th} gazelle. So far, it is determined as the optimal solution, which is approximate in each iteration. Therefore, the process continues until the optimal features are selected. The output of the feature selection phase is symbolized as ζ_e .

3.8 Classification

Lastly, the selected optimal features (ζ_e) are fed into the NC-ELM classifier for classifying diseases and pests. A feed-forward neural network with single or multiple hidden nodes is named ELM. These hidden nodes might be assigned at random and never updated. Conversely, the ELM model might require the hidden layer's higher complexity owing to the random initialization of parameters. This reduces the ELM's robustness for encountering variations in the input data. Hence, the parameter initialization is carried out grounded on the correlated learning rate, which controls the network performance. Moreover, ReLu activation in ELM is replaced with a Non-monotonic function, which effectively improves the parameter learning process and improves the performance of ELM. Figure 3 displays the structure of the NC-ELM classifier.

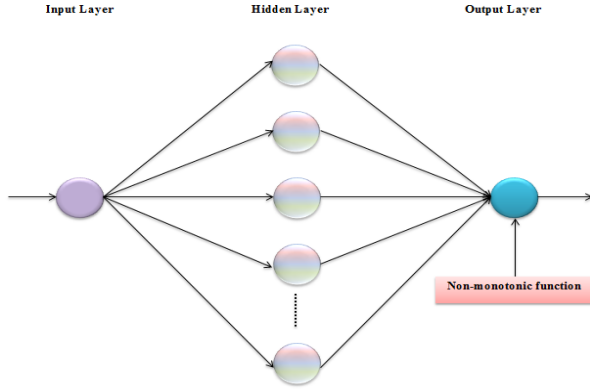


Figure 3: Structure for NC-ELM classifier

Generally, the selected features are given to the input layer. In that, the classifier parameters are initialized using a correlated learning rate, and are given as,

$$d = q \frac{\left(1 + \frac{1}{v}\right)^v}{m} \quad (25)$$

Where, q symbolizes the constant, d is the correlated learning rate, v implies the number of iterations, and m exemplifies the uniform distribution. In that, the hidden layer output can be expressed as,

$$\mathcal{I}\mathcal{R}_c = \mathbf{X} \quad (26)$$

Where, \mathbf{I} is the hidden layer output matrix, \mathcal{R}_c is the weight matrix of the output layer, and \mathbf{X} signifies the target matrix. In the optimization version of ELM, the two parameters $\|\mathbf{I}\beta - \mathbf{X}\|^2$ and $\|\beta\|^2$ are to be minimized. Therefore, the non-monotonic function is utilized as an activation function in the output layer (Φ), and it is mathematically represented as,

$$\Phi = \left[\frac{1}{2} \|\mathcal{R}_c\|^2 + R \frac{1}{2} \sum_{i=1}^G \|\tau_i\|^2 \right] \wp_{nm} \quad (27)$$

$$\wp_{nm} = \mathbf{I} \tanh(\ln(1 + e^1)) \quad (28)$$

Where, the output nodes' training error vector is notated as τ_i , \wp_{nm} signifies the non-monotonic function, and the penalty factor that represents the tradeoff betwixt the minimization of training errors and the maximization of generality ability is exemplified as R . Hence, the proposed NC-ELM successfully classifies the various sorts of leaf diseases, namely Wheat Powdery mildew, Wheat leaf rust, Wheat foliage, Black rust, and Leaf blight, and pests, namely Wheat midges, Hessian

fly, Wheat stem, Cereal leaf beetle, and Cutworms using NC-ELM classifier in the output layer.

Therefore, the pests and disease classification process was performed successfully using the NC-ELM classifier. Hence, to prove the effectiveness of the model, the evaluation of this proposed methodology is necessary. Thus, the result section is explained in the below section.

4. RESULT AND DISCUSSION

Here, the proposed technique is contrasted and analyzed with the existing systems. The publically available dataset is taken for the proposed approach. The working platform for this proposed mechanism is PYTHON. Figure 4 elucidates the proposed research technique's sample image outcomes.

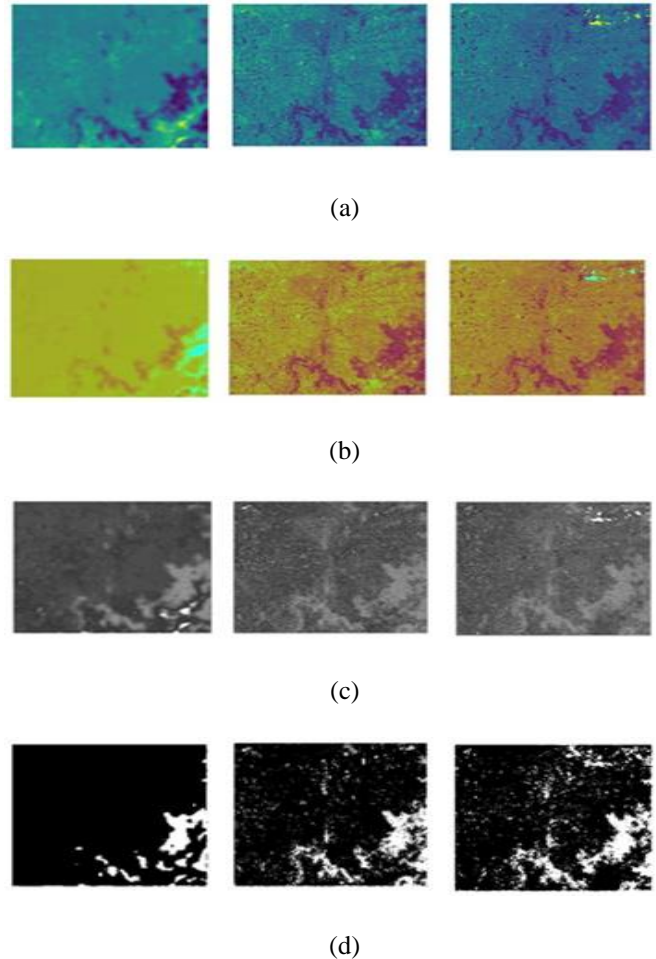


Figure 4: Samples images of (a) Input images (b) Filtered images (c) Region segmented images, and (d) Pest masked images of the proposed methodology

4.1 Performance Analysis

Here, the outcomes are analyzed in 4 segments, namely classification, region segmentation, Feature selection, and Filtering.

Figure 5 displays the count vs. month analysis of disease and pest for the proposed framework.

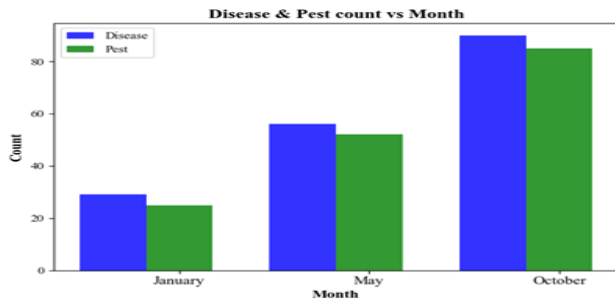


Figure 5: Count vs. Month analysis for the proposed framework

The graphical representation displays that the counting of disease and pest count increases rapidly for all the upcoming months. In the month of January, the count of diseases and pests is approximately 30 and 24. For the same location in the month of May, the count of disease and pest increases. Owing to the growth of plants, the disease and pests are visible, so the count also increases. Likewise, in the month of October, the count increases rapidly. Therefore, the proposed framework is good at detecting diseases and pests.

4.1.1 Performance Evaluation of Classification

Here, the proposed NC-ELM's performance is assessed in comparison with the existing algorithms like Recurrent Neural Network (RNN), Deep Neural Network (DNN), Extreme Learning Machine (ELM), and Convolutional Neural Network (CNN) concerning Precision, Sensitivity, Accuracy, F-Measure, Specificity, along with Training time.

Table 1: Performance analysis for the proposed NC-ELM with the existing algorithms

Algorithms	Accuracy (%)	Precision (%)	F-Measure (%)	Sensitivity (%)	Specificity (%)
Proposed NC-ELM	97.674	98.437	98.437	98.4375	95.454
ELM	94.186	96.825	96.062	94.186	90.909
RNN	91.860	94.915	94.117	93.333	88.461
CNN	89.534	95.081	92.8	90.625	86.363
DNN	87.209	90.909	91.603	92.307	71.428

The proposed NC-ELM's performance assessment with the existing algorithms is depicted in Table 1. The above metrics determine the system's perfectness in classifying diseases and pests. Here, it is clear that the DNN algorithm displays poor performance of 87.2093%, 90.90909%, 91.60305%,

92.30769%, and 71.42857% for accuracy, precision, F-Measure, sensitivity, and specificity, correspondingly. However, the proposed NC-ELM obtained better outcomes in all the metrics during experimental analysis. This shows that with NC-ELM, the disease along with pests is classified more perfectly because of NC, which makes it more suitable for the proposed methodology.

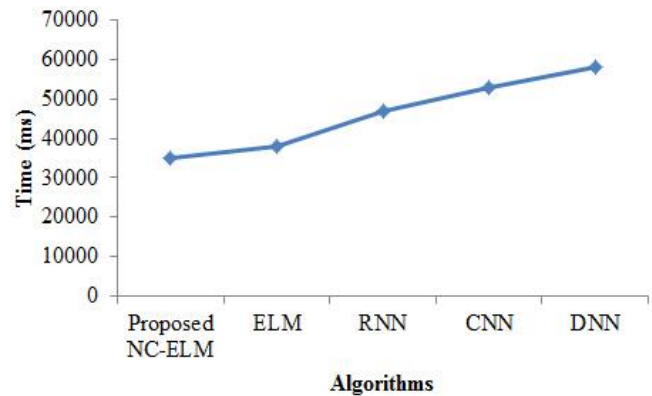


Figure 6: Training time analysis

Training time analysis is performed for the proposed NC-ELM and existing algorithms, which are revealed in Figure 6. Training is necessary to classify the disease and pests of wheat leaves. For that, the proposed NC-ELM obtains the lowest training time of 35006ms among all the existing algorithms. Existing DNN attains the lowest training time followed by existing CNN. Therefore, the training time for the proposed NC-ELM is good owing to the process of correlated function.

4.2 Comparative Analysis

Here, the proposed NC-ELM framework is compared with related works like (T. Zhang et al., 2022), (N. Zhang et al., 2019), (Huang et al., 2020), and (Chen et al., 2018) in terms of accuracy.

Table 2: Comparative analysis in terms of accuracy

Models	Accuracy (%)
Proposed NC-ELM	97.67442
(T. Zhang et al., 2022)	96.93
(N. Zhang et al., 2019)	89.80
(Huang et al., 2020)	92
(Chen et al., 2018)	93.60

The proposed classifier's accuracy analysis in comparison with existing models is illustrated in Table 5. Accuracy is the metric for evaluating the perfectness of the NC-ELM algorithm. Here, the accuracy of the (T. Zhang et al., 2022) is superior to the other conventional frameworks. But, the proposed NC-ELM produces 0.76 % more accuracy than all the

existing models. This improvement in accuracy is owing to the implementation of non-monotonic correlation in the ELM.

5. CONCLUSION

This work proposed the DL model for wheat field disease and pest classification using NC-ELM. Here, AIS is utilized for region segmentation, and WSRT is wielded for filtering. In the experimental analysis, the proposed NC-ELM attains a higher accuracy (97.67442%) among the existing algorithms. Concerning specificity, the proposed NC-ELM attains 95.45455%, which is 7.905% higher than the conventional techniques. In segmentation, the proposed AIS attain the dice score value of 0.702733 owing to the implementation of adaptive irregular modules. The proposed PG-GOA attains a feature selection time of 15965ms, which is 4193 ms lower than the existing methodologies. Because of the SR coefficient, a good PSNR value is attained by the proposed one. Here, owing to the deficiency of particular location images, only a limited number of satellite images are utilized. Moreover, the percentage of disease samples was very lower, which results in data imbalance. In the future, the above limitations will be solved by utilizing data augmentation and data balancing techniques.

REFERENCES

- Justesen, A. F., Corsi, B., Ficke, A., Hartl, L., Holdgate, S., Jørgensen, L. N., et al. (2021). Hidden in plain sight: a molecular field survey of three wheat leaf blotch fungal diseases in North-Western Europe shows co-infection is widespread. *European Journal of Plant Pathology*, 160(4), 949–962. <https://doi.org/10.1007/s10658-021-02298-5>
- Atta, B. M., Saleem, M., Ali, H., Bilal, M. & Fayyaz, M. (2020). Application of Fluorescence Spectroscopy in Wheat Crop: Early Disease Detection and Associated Molecular Changes. *Journal of Fluorescence*, 30(4), 801–810. <https://doi.org/10.1007/s10895-020-02561-8>
- Obaid-Ur-Rehman, Ishaq, R. A. F., Shah, S. R. A. & Shabbir, Y. (2021). UAV Assessment of Crop Evapo-transpiration Dynamics in Winter Wheat and Barley under Varying Pressures of Fungal Diseases. 7th International Conference on Aerospace Science and Engineering (ICASE 2021), October 2022. <https://doi.org/10.1109/ICASE54940.2021.9904260>
- Afrasiabian, Y., Noory, H., Mokhtari, A., Nikoo, M. R., Pourshakouri, F. & Haghighatmehr, P. (2015). Effects of spatial, temporal, and spectral resolutions on the estimation of wheat and barley leaf area index using multi- and hyper-spectral data (case study: Karaj, Iran). *Precision Agriculture*, 22(3), 660–688. <https://doi.org/10.1007/s11119-020-09749-9>
- Zhang, L., Geng, M., Zhang, Z., Zhang, Y., Yan, G., Wen, S., et al. (2020). Molecular mapping of major QTL conferring resistance to orange wheat blossom midge (*Sitodiplosis mosellana*) in Chinese wheat varieties with selective populations. *Theoretical and Applied Genetics*, 133(2), 491–502. <https://doi.org/10.1007/s00122-019-03480-4>
- Rollar, S., Serfling, A., Geyer, M., Hartl, L., Mohler, V. & Ordon, F. (2021). QTL mapping of adult plant and seedling resistance to leaf rust (*Puccinia triticina* Eriks.) in a multiparent advanced generation intercross (MAGIC) wheat population. *Theoretical and Applied Genetics*, 134(1), 37–51. <https://doi.org/10.1007/s00122-020-03657-2>
- Paul, S. K., Mahmud, N. U., Gupta, D. R., Rani, K., Kang, H., Wang, G. L., et al. (2022). *Oryzae* pathotype of *Magnaporthe oryzae* can cause typical blast disease symptoms on both leaves and spikes of wheat under a growth room condition. *Phytopathology Research*, 4(1). <https://doi.org/10.1186/s42483-022-00114-4>
- Kasinathan, T. & Uyyala, S. R. (2021). Machine learning ensemble with image processing for pest identification and classification in field crops. *Neural Computing and Applications*, 33(13), 7491–7504. <https://doi.org/10.1007/s00521-020-05497-z>
- Furbank, R. T., Silva-Perez, V., Evans, J. R., Condon, A. G., Estavillo, G. M., He, W., et al. (2021). Wheat physiology predictor: predicting physiological traits in wheat from hyperspectral reflectance measurements using deep learning. *Plant Methods*, 17(1), 1–15. <https://doi.org/10.1186/s13007-021-00806-6>
- Bouguettaya, A., Zazour, H., Kechida, A. & Taberkit, A. M. (2022). A survey on deep learning-based identification of plant and crop diseases from UAV-based aerial images. *Cluster Computing*, 0123456789. <https://doi.org/10.1007/s10586-022-03627-x>
- Zhang, T., Yang, Z., Xu, Z. & Li, J. (2022). Wheat Yellow Rust Severity Detection by Efficient DF-UNet and UAV Multispectral Imagery. *IEEE Sensors Journal*, 22(9), 9057–9068. <https://doi.org/10.1109/JSEN.2022.3156097>
- Zhang, N., Pan, Y., Feng, H., Zhao, X., Yang, X., Ding, C., et al. (2019). Development of *Fusarium* head blight classification index using hyperspectral microscopy images of winter wheat spikelets. *Biosystems Engineering*, 186, 83–99. <https://doi.org/10.1016/j.biosystemseng.2019.06.008>
- Ren, Y., Huang, W., Ye, H., Zhou, X., Ma, H., Dong, Y., et al. (2021). Quantitative identification of yellow rust in winter wheat with a new spectral index: Development and validation using simulated and experimental data. *International Journal of Applied Earth Observation and Geoinformation*, 102, 102384. <https://doi.org/10.1016/j.jag.2021.102384>
- Huang, L., Li, T., Ding, C., Zhao, J., Zhang, D. & Yang, G. (2020). Diagnosis of the severity of *Fusarium* head blight of wheat ears on the basis of image and spectral feature fusion. *Sensors (Switzerland)*, 20(10). <https://doi.org/10.3390/s20102887>
- Chen, D., Shi, Y., Huang, W., Zhang, J. & Wu, K. (2018). Mapping wheat rust based on high spatial resolution satellite imagery. *Computers and Electronics in Agriculture*, 152(September 2017), 109–116. <https://doi.org/10.1016/j.compag.2018.07.002>
- Wang, X., Liu, C. & van der Fels-Klerx, H. J. (2022). Regional prediction of multi-mycotoxin contamination of wheat in Europe using machine learning. *Food Research International*, 159(June), 111588. <https://doi.org/10.1016/j.foodres.2022.111588>
- Qiu, R., Yang, C., Moghimi, A., Zhang, M., Steffenson, B. J. & Hirsch, C. D. (2019). Detection of *Fusarium* Head Blight in wheat using a deep neural network and color imaging. *Remote Sensing*, 11(22). <https://doi.org/10.3390/rs11222658>
- Hu, P., Yang, W., Wang, X. & Mao, S. (2022). Contact-free wheat mildew detection with commodity wifi. *International Journal of Cognitive Computing in Engineering*, 3(January), 9–23. <https://doi.org/10.1016/j.ijcce.2022.01.001>
- Kang, H., Peng, Y., Hua, K., Deng, Y., Bellizzi, M., Gupta, D. R., et al. (2021). Rapid Detection of Wheat Blast Pathogen *Magnaporthe oryzae* Triticum Pathotype Using Genome-Specific Primers and Cas12a-mediated Technology. *Engineering*, 7(9), 1326–1335. <https://doi.org/10.1016/j.eng.2020.07.016>
- Li, R., Jia, X., Hu, M., Zhou, M., Li, D., Liu, W., et al. (2019). An Effective Data Augmentation Strategy for CNN-Based Pest Localization and Recognition in the Field. *IEEE Access*, 7, 160274–160283. <https://doi.org/10.1109/ACCESS.2019.2949852>
- Justesen, A. F., Corsi, B., Ficke, A., Hartl, L., Holdgate, S., Jørgensen, L. N., et al. (2021). Hidden in plain sight: a molecular field survey of three wheat leaf blotch fungal diseases in North-Western Europe shows co-infection is widespread. *European Journal of Plant Pathology*, 160(4), 949–962. <https://doi.org/10.1007/s10658-021-02298-5>
- Atta, B. M., Saleem, M., Ali, H., Bilal, M. & Fayyaz, M. (2020). Application of Fluorescence Spectroscopy in Wheat Crop: Early Disease Detection and Associated Molecular Changes. *Journal of Fluorescence*, 30(4), 801–810. <https://doi.org/10.1007/s10895-020-02561-8>
- Obaid-Ur-Rehman, Ishaq, R. A. F., Shah, S. R. A. & Shabbir, Y. (2021). UAV Assessment of Crop Evapo-transpiration Dynamics in Winter Wheat and Barley under Varying Pressures of Fungal Diseases. 7th International Conference on Aerospace Science and Engineering (ICASE 2021), October 2022. <https://doi.org/10.1109/ICASE54940.2021.9904260>

24. Afrasiabian, Y., Noory, H., Mokhtari, A., Nikoo, M. R., Poursakouri, F. & Haghighatmehr, P. (2015). Effects of spatial, temporal, and spectral resolutions on the estimation of wheat and barley leaf area index using multi- and hyper-spectral data (case study: Karaj, Iran). *Precision Agriculture*, 22(3), 660–688. <https://doi.org/10.1007/s11119-020-09749-9>
25. Zhang, L., Geng, M., Zhang, Z., Zhang, Y., Yan, G., Wen, S., et al. (2020). Molecular mapping of major QTL conferring resistance to orange wheat blossom midge (*Sitodiplosis mosellana*) in Chinese wheat varieties with selective populations. *Theoretical and Applied Genetics*, 133(2), 491–502. <https://doi.org/10.1007/s00122-019-03480-4>
26. Rollar, S., Serfling, A., Geyer, M., Hartl, L., Mohler, V. & Ordon, F. (2021). QTL mapping of adult plant and seedling resistance to leaf rust (*Puccinia triticina* Eriks.) in a multiparent advanced generation intercross (MAGIC) wheat population. *Theoretical and Applied Genetics*, 134(1), 37–51. <https://doi.org/10.1007/s00122-020-03657-2>
27. Paul, S. K., Mahmud, N. U., Gupta, D. R., Rani, K., Kang, H., Wang, G. L., et al. (2022). *Oryzae* pathotype of *Magnaporthe oryzae* can cause typical blast disease symptoms on both leaves and spikes of wheat under a growth room condition. *Phytopathology Research*, 4(1). <https://doi.org/10.1186/s42483-022-00114-4>
28. Kasinathan, T. & Uyyala, S. R. (2021). Machine learning ensemble with image processing for pest identification and classification in field crops. *Neural Computing and Applications*, 33(13), 7491–7504. <https://doi.org/10.1007/s00521-020-05497-z>
29. Furbank, R. T., Silva-Perez, V., Evans, J. R., Condon, A. G., Estavillo, G. M., He, W., et al. (2021). Wheat physiology predictor: predicting physiological traits in wheat from hyperspectral reflectance measurements using deep learning. *Plant Methods*, 17(1), 1–15. <https://doi.org/10.1186/s13007-021-00806-6>
30. Bouguettaya, A., Zarzour, H., Kechida, A. & Taberkit, A. M. (2022). A survey on deep learning-based identification of plant and crop diseases from UAV-based aerial images. *Cluster Computing*, 0123456789. <https://doi.org/10.1007/s10586-022-03627-x>
31. Zhang, T., Yang, Z., Xu, Z. & Li, J. (2022). Wheat Yellow Rust Severity Detection by Efficient DF-UNet and UAV Multispectral Imagery. *IEEE Sensors Journal*, 22(9), 9057–9068. <https://doi.org/10.1109/JSEN.2022.3156097>
32. Zhang, N., Pan, Y., Feng, H., Zhao, X., Yang, X., Ding, C., et al. (2019). Development of *Fusarium* head blight classification index using hyperspectral microscopy images of winter wheat spikelets. *Biosystems Engineering*, 186, 83–99. <https://doi.org/10.1016/j.biosystemseng.2019.06.008>
33. Ren, Y., Huang, W., Ye, H., Zhou, X., Ma, H., Dong, Y., et al. (2021). Quantitative identification of yellow rust in winter wheat with a new spectral index: Development and validation using simulated and experimental data. *International Journal of Applied Earth Observation and Geoinformation*, 102, 102384. <https://doi.org/10.1016/j.jag.2021.102384>
34. Huang, L., Li, T., Ding, C., Zhao, J., Zhang, D. & Yang, G. (2020). Diagnosis of the severity of *Fusarium* head blight of wheat ears on the basis of image and spectral feature fusion. *Sensors (Switzerland)*, 20(10). <https://doi.org/10.3390/s20102887>
35. Chen, D., Shi, Y., Huang, W., Zhang, J. & Wu, K. (2018). Mapping wheat rust based on high spatial resolution satellite imagery. *Computers and Electronics in Agriculture*, 152(September 2017), 109–116. <https://doi.org/10.1016/j.compag.2018.07.002>
36. Wang, X., Liu, C. & van der Fels-Klerx, H. J. (2022). Regional prediction of multi-mycotoxin contamination of wheat in Europe using machine learning. *Food Research International*, 159(June), 111588. <https://doi.org/10.1016/j.foodres.2022.111588>
37. Qiu, R., Yang, C., Moghimi, A., Zhang, M., Steffenson, B. J. & Hirsch, C. D. (2019). Detection of *Fusarium* Head Blight in wheat using a deep neural network and color imaging. *Remote Sensing*, 11(22). <https://doi.org/10.3390/rs11222658>
38. Hu, P., Yang, W., Wang, X. & Mao, S. (2022). Contact-free wheat mildew detection with commodity wifi. *International Journal of Cognitive Computing in Engineering*, 3(January), 9–23. <https://doi.org/10.1016/j.ijcce.2022.01.001>
39. Kang, H., Peng, Y., Hua, K., Deng, Y., Bellizzi, M., Gupta, D. R., et al. (2021). Rapid Detection of Wheat Blast Pathogen *Magnaporthe oryzae* Triticum Pathotype Using Genome-Specific Primers and Cas12a-mediated Technology. *Engineering*, 7(9), 1326–1335. <https://doi.org/10.1016/j.eng.2020.07.016>
40. Li, R., Jia, X., Hu, M., Zhou, M., Li, D., Liu, W., et al. (2019). An Effective Data Augmentation Strategy for CNN-Based Pest Localization and Recognition in the Field. *IEEE Access*, 7, 160274–160283. <https://doi.org/10.1109/ACCESS.2019.2949852>

Authors



Lakshmi Priya S completed her ME degree in Big Data Analytics from Anna University, Guindy, Chennai, India in 2020. She is currently pursuing PhD at the Department of Computer Science and Engineering, Sathyabama Institute of Science and Technology, Tamil Nadu, India. Her areas of interest are Artificial Intelligence, Machine Learning, Natural Language Processing, and Data Science.

Email: lpriya0204@gmail.com



R Subhashini, currently working as Professor and Head in the Department of Information Technology, Sathyabama Institute of Science and Technology. She has two decades of teaching and research experience. She was awarded the Degree of Philosophy from the Faculty of Computing, Sathyabama Institute of Science and Technology in the year 2012. Her research interests are big data, Data mining, Image processing, Machine Learning, Artificial Intelligence and distributed computing. She has been involved in various Consultancy project developments. She has received funding from DST and established the DST – FIST funded Cloud Computing lab in the year 2015. Also received funds from various government agencies like DST, DRDO, CSIR and AICTE and organized International Conferences, FDPs and Workshops. She has published more than 200 research papers in various International Journals and Conferences. She is an Associate Editor in the International Journal of Information Retrieval and Research.

Email: subaagopi@gmail.com